Diffractive processes at high energies.

Abramovsky V.A.*, Dmitriev A.V.†, Shneider A.A.

Novgorod State University, B. S.-Peterburgskaya Street 41,

Novgorod the Great, Russia, 173003

April 29, 2005

Abstract

In this work we calculate pomeron flux in the single diffraction processes. We consider two models: quasi-eikonal model and low constituent model. Both models give the pictures different from the traditional three-reggeon model. Successive developing of modeles gives some indications, that the low constituent model is more attractive.

1 Introduction

Regge non-enhanced phenomenology well describes total and elastic cross-sections in the Donnachie-Landshoff parametrization [1], see figures in [3] and [2].

Low-energy single diffraction data is also well described by regge phenomenology with supercritical pomeron, but at the region of Tevatron energies it fails to describe data on single diffraction dissociation. The main problem is that total single diffraction cross-section rise considerably weaker than it is predicted by Y-like Regge diagrams involving only three pomerons. This fact was clearly stated by Goulianos, see [7] and references within.

Many ways were suggested to solve this problem. First way is two-variant (Ref.[7] and Ref.[8]) pomeron flux renormalization model, where we consider the equation for cross section of single diffraction

$$\frac{d^3\sigma}{dM^2dt} = f_{I\!P/p}(x,t)\sigma_{I\!Pp}(s) \tag{1}$$

and pick out the factor, named as 'pomeron flux'

$$f_{I\!P/p}(x,t) = K\xi^{1-2\alpha_{I\!P}(t))} \tag{2}$$

Renormalization of the pomeron flux is made by intserting dependence of K either on s (as in Ref.[7]) either on x,t, as in Ref.[8]. This phenomenological approach well describes CDF data on single diffraction, but we need more theoretical bases for extrapolation to higher energies.

*ava@novsu.ac.ru

†gridlab@novsu.ac.ru

The second way is straight-forward account of screening corrections (Ref.[6] and Ref.[9]). This way seems to be more natural, but we need to introduce additional parameters and make some assumptions about Regge diagram technics. In Ref.[6] and Ref.[9] only some parts of sufficient diagrams were accounted by going to the impact parameter space b and replacement initial "Borhn" factor $\chi(s,\overline{b})$ to eikonalized amplitude $(1 - e^{-\mu\chi(s,\overline{b})})$. In addiction, the central Y-like diagram was modified to account low-energy processes and in Ref.[9] the dependence of pomeron intercept on energy was introduced.

As compared with Ref.[6] and Ref.[9] we successivly consider all non-enhanced diagrams.

In this work we also consider low constituent model, where there is only basic quark-gluon states and interactions. This model leads us to the non-local pomeron, but it has clear interpretation of the pomeron flux.

2 Quasi-eikonal model

Quasi-eikonal model, considered in this work, is standart enough. We use reggeon diagram technic with reggeon propogator $s^{\alpha(t)}$, model gauss vertexes of the interaction of n pomerons with hadron

$$N_h(k_1,..,k_n) = g_h(g_h c_h)^{n-1} exp\left(-R_h^2 \sum_{i=1}^{n} k_i^2\right) \tag{3}$$

and the vertex corresponding to the transition of l pomerons into m pomerons under the π -meson exchange dominance assumption

$$\Lambda(k_1,..,k_m) = r(g_\pi c_\pi)^{m-3} exp\left(-R_r^2 \sum_{i=1}^{m} k_i^2\right). \tag{4}$$

Here g_h is the pomeron-hadron coupling, c_h is the corresponding shower enhancement coefficient, R_h and R_r are the radii of the pomeron-hadron and pomeron-pomeron interactions, respectively, k_i are the pomeron transverse momenta. Integration on the pomeron momenta is made trivial in the impact parameter space represenztation and we only have to sum on then nubmers of pomerons, attached to the same vertexes.

As compared with Ref.[6] and Ref.[9], where only part of sufficient diagrams was accounted (see Fig. 1a), in this paper we account all non-enhanced absorptive corrections to the Y-diagram contribution, shown in Fig.1b.

Because low-energy corrections rapidly decrease with energy, we account only pomeron contributions, but in all sufficient diagrams, as it was done in Ref.[10] and Ref.[11]. It gives us possibility to normalize cross-section of the single diffraction to CDF data and make theoreticaly based predictions for cross-section of the single diffraction at LHC energies.

The contribution $f_{n_1 n_2 n_3 n_4 n_5}$ of each diagram in Fig.1b can be written in a *rather simple form*

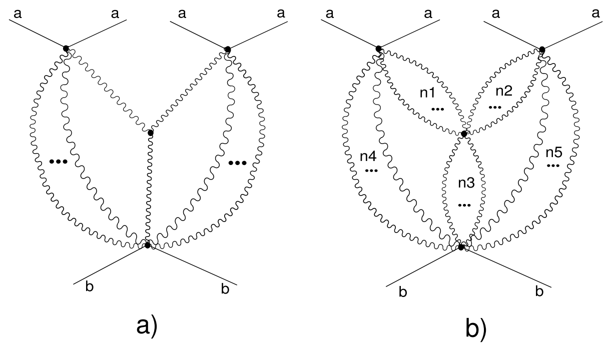

Figure 1: Regge diagrams describing single diffraction dissociation of particle b.

$$\begin{aligned}
f_{n_1 n_2 n_3 n_4 n_5} &= \frac{(-1)^{n_1+n_2+n_3+n_4+n_5+1}}{n_1!n_2!n_3!n_4!n_5!}\frac{8\pi^3 r}{c_a^2 c_b g_\pi c_\pi} \\
&\times \left[\frac{g_a c_a g_\pi c_\pi e^{\Delta(Y-y)}}{8\pi(R_a^2+R_\pi^2+\alpha'(Y-y))}\right]^{n1+n2} \\
&\times \left[\frac{g_a c_a g_b c_b e^{\Delta Y}}{8\pi(R_a^2+R_b^2+\alpha' Y)}\right]^{n4+n5}\left[\frac{g_b c_b g_\pi c_\pi e^{\Delta y}}{8\pi(R_b^2+R_\pi^2+\alpha' y)}\right]^{n3} \\
&\times \frac{1}{detF} e^{-t\frac{c}{detF}} \\
detF &= a_1a_2a_3 + a_1a_3a_5 + a_1a_2a_5 + a_1a_2a_4 \\
&+ a_2a_3a_4 + a_1a_4a_5 + a_3a_4a_5 + a_2a_4a_5
\end{aligned}$$

$$c = a_2a_3 + a_1a_5 + a_3a_5 + a_2a_5 + a_1a_3 + a_1a_4 + a_3a_4 + a_2a_4$$

$$a_1 = \frac{n_1}{R_a^2+R_\pi^2+\alpha'(Y-y)};\ \ a_2 = \frac{n_2}{R_a^2+R_\pi^2+\alpha'(Y-y)};\ \ a_3 = \frac{n_3}{R_b^2+R_\pi^2+\alpha' y}$$

$$a_4 = \frac{n_4}{R_a^2+R_b^2+\alpha' Y};\ \ a_5 = \frac{n_5}{R_a^2+R_b^2+\alpha' Y}$$

Here $Y = ln(s)$ $y = ln(M^2)$. Then inclusive cross section is

$$(2\pi)^3 2E\frac{d^3\sigma}{dp^3} = \pi\frac{s}{M^2}\sum_{n_1,n_2,n_3=1}^{\infty}\sum_{n_4,n_5=0}^{\infty} f_{n_1n_2n_3n_4n_5} \tag{5}$$

Our method differs from early work Ref. [11], where all parameters but vertex r were fixed. In this work here we vary all parameters. Parameters were varied with natural limitations, i.e. all parameters were varied above its conventional values. We don‘t consider very high or very low values of pomeron itercept and slope, which can be compensated by other parameters.

Another difference as compared with Ref.[11] is the fact, that we use data on total and elestic (differential) cross-sections and data on total single-diffraction cross-sections. So, we can fix parameters of the model with higher precision and with account of its one-to-one corellations.

The model under consideration doesn‘t include possible contributions of low-lying reggeons, so we limit considered energies by $\sqrt{s} > 52GeV$ for elastic and total cross-sections. As was shown in [13], modern data don't give us possibility to distinct simple ploe model with total cross-sections $\sigma_{tot} = As^{\Delta}$ and eikonaliezed models with $\sigma_{tot} = C + Dln(s)$ or $\sigma_{tot} = E + Fln(s)^2$. But we can reliably determine parameters of the model $R_h, g_h, \Delta, \alpha'$ from elastic and total cross-section data at fixing c_h.

We use CDF data on single diffraction for analysis.

CDF data [4] was presented as a result of the monte-carlo simulations based on the general formula:

$$\begin{array}{l} \frac{d^2\sigma}{d\xi dt} = \frac{1}{2}\left[\frac{D}{\xi^{1+\epsilon}} e^{(b_0 - 2\alpha'_{SD}\ln\xi)t} + I\xi^{\gamma} e^{b't}\right] \\ \xi \equiv 1 - x \end{array} \qquad (6)$$

Taken CDF data is shown in Table 1.

Table 1: CDF fit-parameters from reference [1].

	$\sqrt{s} = 546\ GeV$	$\sqrt{s} = 1800\ GeV$
D	3.53 ± 0.35	2.54 ± 0.43
b_0	7.7 ± 0.6	4.2 ± 0.5
α'_{SD}	0.25 ± 0.02	0.25 ± 0.02
ϵ	0.121 ± 0.011	0.103 ± 0.017
I	537^{+498}_{-280}	162^{+160}_{-85}
γ	0.71 ± 0.22	0.1 ± 0.16
b'	10.2 ± 1.5	7.3 ± 1.0

This parameters are experimental points tested in our model. Let's mark, that low-lying reggeons contribution, corresponding to second addendum in (6), isn't acconted in our calculations and we have to model only parameters D,b_0,α'_{SD},ϵ. We calculate this parameters in the region

$$0.05 < t < 0.1; 0.99 < x < 0.995 ,$$

where we have the most reliable CDF data and contribution of the low-lying reggeons is mnimal.

We have to mark, that this data is not precise because of the following reasons:

1. CDF single diffraction data have low statistcs and narrow kinematical region, where the data was taken;
2. At each energy ($\sqrt{s} = 546GeV \quad \sqrt{s} = 1800GeV$) 6 highly correlated parameters are introduced, and it makes calculations unstable;

3. Fixing of effective pomeron slope on the common value $\alpha'_{SD} = 0.25$ is obliged.

Unreability of the data in Table1 is cearly seen from analysis of dependence of D on energy from $\sqrt{s} = 546GeV$ to $\sqrt{s} = 1800GeV$. As defined [4],

$$D = G(0)s^{\Delta} \tag{7}$$

here G(0) doesn't depend on s, and $\Delta > 0$. In accordance with this definition, parameter D must increase when energy increases, but in CDF data it decreases.

Total single diffraction cross-sections are well experimentally defined and don't depend on the model, used in analysis of basic data (detectors counts)

$$\begin{aligned} \sigma_{SD}(\sqrt{s} = 546GeV) = 7.89 \pm 0.33mb \\ \sigma_{SD}(\sqrt{s} = 1800GeV) = 9.46 \pm 0.44mb \end{aligned} \tag{8}$$

We include these two points in χ^2 test, but with larger weights, than points shown in Table 1.

Because total and elastic cross sections, on one side, and single diffraction cross sections, on other side, have different types, we vary parameters r,R_π and c_π to achieve the best agreement with data in Table1 and data (8), fixing at each step parameters Δ,α',g_h and R_h from total and elastic cross-sections.

Results. In the end of optimization process we've got next parameter set: $g_p^2 = 75.0538, \Delta = 0.0868089, R_p^2 = 1.94755, \alpha\prime = 0.148963, c_p^2 = 2.03954,$
$r = 0.111525, R_\pi^2 = 0.173682, c_\pi^2 = 6.00989$

Following total single diffraction cross sections were calculated at these parameters:

$$\begin{aligned} \sigma_{SD}(\sqrt{s} = 546GeV) = 7.5mb \\ \sigma_{SD}(\sqrt{s} = 1800GeV) = 10mb \end{aligned} \tag{9}$$

Corresponding differential characteristics of differential single diffraction cross sections are enumerated in Table 2:

Calculated differential characteristics are very close to ones from the triple-pomerom model, so the following relation is satisfied

$$\frac{d^3\sigma}{dM^2dt} = f_{I\!P/p}(x,t)\sigma_{I\!Pp}(s) \tag{10}$$

where

$$f_{I\!P/p}(x,t) = K(s)\xi^{1-2\alpha_{I\!P}(t))} \tag{11}$$

is renormalized pomeron flux. As compared with standart triple-pomeron model the dependence of factor K on ernergy s is introduced. This dependence provides slowing on the rise of the single diffraction cross section with energy.

Dependence of renormalizing factor $K(s)$ on energy is shown on Fig.2.

We have to note, that we have inconsistences that calculating c_p. From one side, there are theoretical indications, that $c_p > 1$. Such high values of c_p lead

Table 2: Differential characteristics of differential single diffraction cross sections in our model.

	$\sqrt{s} = 546\ GeV$	$\sqrt{s} = 1800\ GeV$
D	2.9628	3.08731
b_0	5.32553	5.27187
α'_{SD}	0.294999	0.270871
ϵ	0.0580572	0.0549202

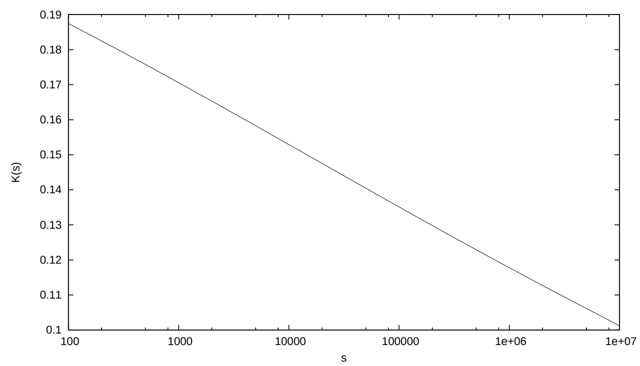

Figure 2: Dependence of renormalizing factor $K(s)$ on energy.

to significant divergence of dependence $\frac{d\sigma}{dt}$ on t from exponential behavior e^{-bt} already at $t{\sim}0.2GeV^2$. It is known from experiment, that elastic cross-section falls exponentially on t up to $t{\sim}1GeV^2$. This inconsistence is clearly seen from Fig.3.

From this fact of independence of logarithmic slope on t we conclude, that $c_p << 1$. To explain slow rise of σ_{SD} with energy we have to assume very high c_π, $c_\pi c_p \gg 1$ at $g_\pi \sim g_p$. It gives desired value of the fraction $\frac{\sigma(\sqrt{s}=1800GeV)}{\sigma(\sqrt{s}=546GeV)} \sim 1.2$, but leads to very high values of logarithmic slope $b \sim 50GeV^{-2}$ (situation will be even more worse, than in the case of elastic cross-section, shown on Fig.3). Solving of this problem by precise adaptation of R_π is unusable, because it leads to highly differing from experiment and depended on M^2 and t values of α' and ϵ.

At $c_p > 1$ we don't need c_π in so high values, and logarithmic slope b is back to values about ones, not tens. So, we must return to the theoretically based area $c_p > 1$ and limit considered area of elastic scattering by $t < 0.2GeV^2$.

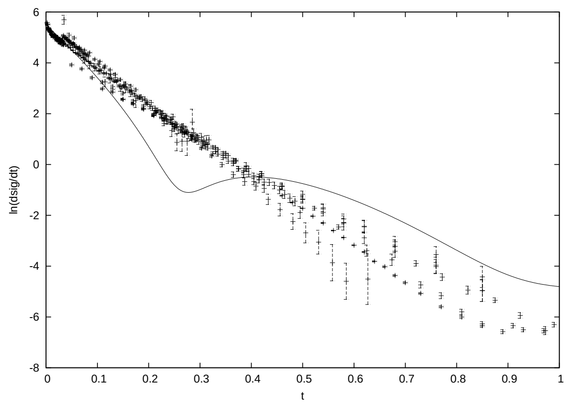

Figure 3: Elastic cross sections $\frac{d\sigma}{dt}$ for reaction $p+p \to p+p$. Theoretical curve is at energy $\sqrt{s} = 1800GeV$. Experimental points are taken at energies from ISR to Tevatron.

We see, that goog agreement of quasi-eikonal model with experiment is achieved on the border of the allowed region of parameters $[c_p, c_\pi]$ (see. Fig.4).

From one side, it gives stability of the calculated parameters. From the other side this model has no reserve of stability. If fraction of the cross sections $\frac{\sigma(\sqrt{s}=1800GeV)}{\sigma(\sqrt{s}=546GeV)}$ will be defined more precisely and will be found in the region $1.1 \div 1.15$ (it is minimal value, which is consistent with existed data), then for description of this data we will be obliged to decline either describing elastic and total cross sections or describing logarithmic slope of the single diffraction on t.

3 Low constituent model

We consider the three-stage model of hadron interaction at the high energies.

On the first stage before the collision there is a small number of partons in hadrons. Their number, basically, coinsides with number of valent quarks and slow increases with the rise of energy owing to the appearance of the breasstralung gluons.

On the second stage the hadron interaction is carried out by gluon exchange between the valent quarks and initial (bremsstralung) gluons and the hadrons gain the colour charge.

On the third step after the interaction the colour hadrons fly away and when the distance between them becomes more than the confinement radius r_c, the lines of the colour electric field gather into the tube of the radius r_c. This tube breaks out into the secondary hadrons.

Because the process of the secondary harons production from colour tube goes with the probability 1, module square of the inelastic amplitudes corre-